



HAL
open science

Statistical Damage Mechanics and Extreme Value Theory

A. Rinaldi, D. Krajcinovic, S. Mastilovic

► **To cite this version:**

A. Rinaldi, D. Krajcinovic, S. Mastilovic. Statistical Damage Mechanics and Extreme Value Theory. International Journal of Damage Mechanics, 2007, 16 (1), pp.57-76. 10.1177/1056789507060779 . hal-00571166

HAL Id: hal-00571166

<https://hal.science/hal-00571166>

Submitted on 1 Mar 2011

HAL is a multi-disciplinary open access archive for the deposit and dissemination of scientific research documents, whether they are published or not. The documents may come from teaching and research institutions in France or abroad, or from public or private research centers.

L'archive ouverte pluridisciplinaire **HAL**, est destinée au dépôt et à la diffusion de documents scientifiques de niveau recherche, publiés ou non, émanant des établissements d'enseignement et de recherche français ou étrangers, des laboratoires publics ou privés.

Statistical Damage Mechanics and Extreme Value Theory

A. RINALDI* AND D. KRAJČINOVIC

*Mechanical and Aerospace Engineering, Arizona State University
Tempe, AZ 85287-6106, USA*

S. MASTILOVIC

*Center for Multidisciplinary Studies, University of Belgrade
Kneza Visislava 1, 11030 Belgrade, Serbia and Montenegro*

ABSTRACT: The statistical damage model presented by the authors in the previous article of this series is used to formulate analytical constitutive relations for the hardening and softening phases of two-dimensional lattices. An alternative approach to the classical damage parameter approach is presented here. A semi-empirical model based on extreme value theory (EVT) is offered.

KEY WORDS: failure, statistical damage mechanics, damage tolerance principles, aircraft worthiness, constitutive relations, extreme value theory, scaling.

INTRODUCTION

Damage Tolerance Principles

MANY ENGINEERING SOLID materials, such as polycrystalline ceramics, metals, and alloys have random microstructure. A microstructure containing many randomly distributed microcracks is initially statistically homogeneous but becomes heterogeneous due to the propagation and clustering of microcracks when a macrocrack forms close to failure. In (Krajcinovic and Rinaldi, 2005a; Rinaldi, et al. 2005), the authors propose constitutive relations obtained from a simple discrete statistical model and discuss the homogeneous to heterogeneous phase transition using

*Author to whom correspondence should be addressed. E-mail: anto@asu.edu and antonio.rinaldi@gmail.com
Figures 2–4, 11 and 12 appear in color online: <http://jfd.sagepub.com>

the analytical tools of statistical mechanics, thermodynamics, and fractal geometry. The threshold of failure depends on the size of the structure and the transformations of the microstructure. The limit states design is driven by crack growth but also by the changes in the microstructure in the heterogeneous phase. The base of structural design and maintenance principles in Boeing Commercial Airplane Group, USA, is the ‘damage tolerance principles’ (Goranson, 1993), which is focused on two structural design objectives: damage tolerance and durability. The former is the ‘ability of the structure to sustain anticipated loads in the presence of fatigue, corrosion or accidental damage until such damage is detected through inspections or malfunctions and repaired’ (Goranson, 1993). The latter is the ‘ability of the structure to sustain degradation from such sources as fatigue, accidental damage, and environmental deterioration to the extent that they can be controlled by economically acceptable maintenance and inspection programs’ (Goranson, 1993).

Damage tolerance is comprised of three elements of importance for achieving the desired level of safety. The first element is the determination of the residual strength or maximum allowable damage (including multiple secondary cracks) that the structure can sustain under regulatory fail-safe load conditions. The second element is the crack growth, defined as the interval of damage progression from lengths with negligible probability of failure to an allowable size determined by the residual strength. Finally, a damage detection strategy (inspection program) must be adopted. The sequence of inspections in a fleet of airplanes requires methods and intervals selected to achieve timely damage detection.

Figure 1 (adopted from (Goranson, 1993)), shows typical experimental data from both full-scale crack growth testing (600 tests on two different wing-panels of width 200 and 2300 mm) and linear elastic fracture mechanics (LEFM). The crack length is normalized to the LEFM limit L_y , and the strengths are normalized to the maximum strength of a pristine undamaged panel. The maximum allowable damage (i.e., the minimum normalized strength) and the corresponding maximum defect length are assigned on such graphs in compliance with a ‘fail-safe’ strategy. Nevertheless, the choice of the tolerable damage is largely based on experience and on the probability of detection (POD) from visual inspections. Full-scale tests are necessary to assess the effect of the structural size on the damage tolerance, but Goranson (1993) recognizes the ‘impossibility’ of conducting full-size fracture and fatigue tests to obtain the data in Figure 1 for all components: ‘The emphasis on residual strength verification has gradually shifted in recent years from wing structures to fuselage pressure shells’ because ‘the extended use of jet transport structures raised concerns about

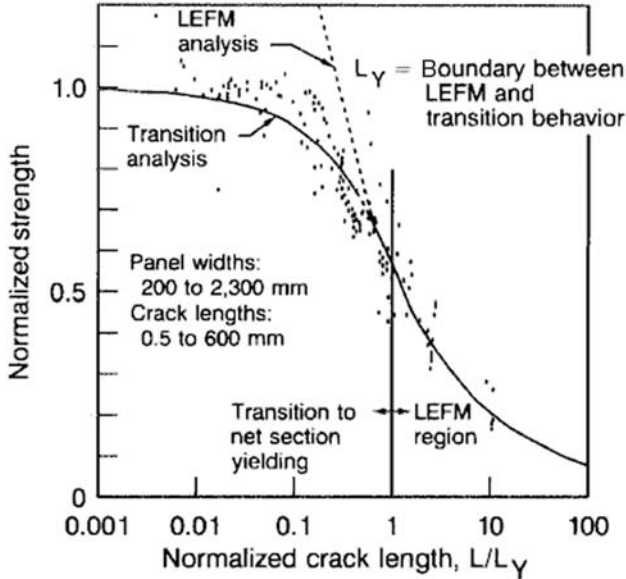


Figure 1. Sample data of crack growth experiments on wing panels used at Boeing Co. (Rinaldi et al., 2005).

multiple site damage in fuselage structures’ (Goranson, 1993), which lead to expensive full-scale tests (of the order of millions of dollars) with large pressure test fixtures. Unfortunately, LEFM is not always applied to multiple-site cracking and diffuse damage, which is nowadays still managed in a purely empirical manner. In conclusion, there is an urge to formulate more reliable multiscale analytical models that account for the structural size effect and that can be used for data extrapolation. The capability of estimating the POD *a priori* from such models is likely to have a deep impact on the fail-safe strategy.

Goranson’s ‘damage tolerance principles’ expresses concern about the ‘lack of interest’ in the scientific community to characterize and quantify the probability of detection. The uniaxial tensile response of two-dimensional disordered spring networks (lattices) is analyzed here. The time-independent damage model (Kachanov, 1958) $\bar{\sigma} = \bar{E}^0(1 - \bar{D})\bar{\epsilon}$, relating the macrostress $\bar{\sigma}$ and the macrostrain $\bar{\epsilon}$ through the damage parameter \bar{D} , was formulated in (Krajcinovic and Rinaldi, 2005a; Rinaldi, et al., 2005). As an alternative to such a constitutive relation based on the damage parameter, this article proposes a semi-empirical constitutive model extracted from numerical data

on the basis of the extreme value theory (EVT). This approach allows scaling the relevant statistics across different lattice sizes.

LATTICE SIMULATIONS AND NUMERICAL DATA

On the microscale, a polycrystalline material in two-dimensional space is similar to a random Voronoi/Delaunay graph (Krajcinovic and Rinaldi, 2005a, b). A Voronoi polygon represents a grain whereas one bond in the Delaunay lattices is representative of a grain boundary. Damage evolution is a stochastic process dependent on the disorder of the microstructure. The lattice is geometrically disordered since the equilibrium distances between particles are normally distributed within the range $\alpha_l \bar{\lambda} \leq \lambda \leq (2 - \alpha_l) \bar{\lambda}$ with $\alpha_l = 0.1$ (if $\alpha_l = 1$, all grains are perfect hexagons). Damage is introduced in the network by the rupturing of the links, which represent intergranular microcrack formation. The links are linear elastic springs with finite random tensile strength and have the same stiffness k . If the critical tensile strain ε_{cr} is reached, permanent rupture occurs and the spring turns into a contact element. The tensile stiffness becomes zero and the link cannot any longer carry tensile forces. Broken springs remain active in compression if load reversal occurs in the course of deformation to account for crack closure. The values ε_{cr} are randomly sampled from a uniform distribution starting at zero. This lattice model considers intergranular microcracks only, which is a reasonable approximation for many ceramics (Davidge, 1979). Since the resolution length of the model is equal to the grain facet, the rupture, i.e., the growth of a microcrack from the initial length to the length of the grain boundary facet, is assumed to be instantaneous.

Quasi-static uniaxial tensile tests are simulated in displacement-controlled conditions on different lattice sizes (Figure 2(a)). The molecular dynamics solver based on the Verlet's algorithm (Krajcinovic and Rinaldi, 2005b; Mastilovic and Krajcinovic, 1999) was adopted. Each simulation is carried incrementally up to the threshold of failure by applying small displacement steps and by computing the equilibrium configuration at each step. The damage process is tracked during the deformation by recording the number of broken bonds, n . The macroscopic data scatter of the \bar{F} versus \bar{u} and n versus \bar{u} curves (within size variability) indicates that $\bar{F}(\bar{u}, L)$ is a random variable at any given \bar{u} in the softening phase (Figure 2(c) and (d)). The average \bar{F} versus \bar{u} and n versus \bar{u} curves from the 10 replicates per size $N = (24, 48, 96, 192)$ were used for the scaling procedure in (Krajcinovic and Rinaldi, 2005a), with N being the number of grains per lattice side. The original dataset is expanded here to enhance the accuracy, robustness, and precision of the regression analysis. Intermediate lattice sizes

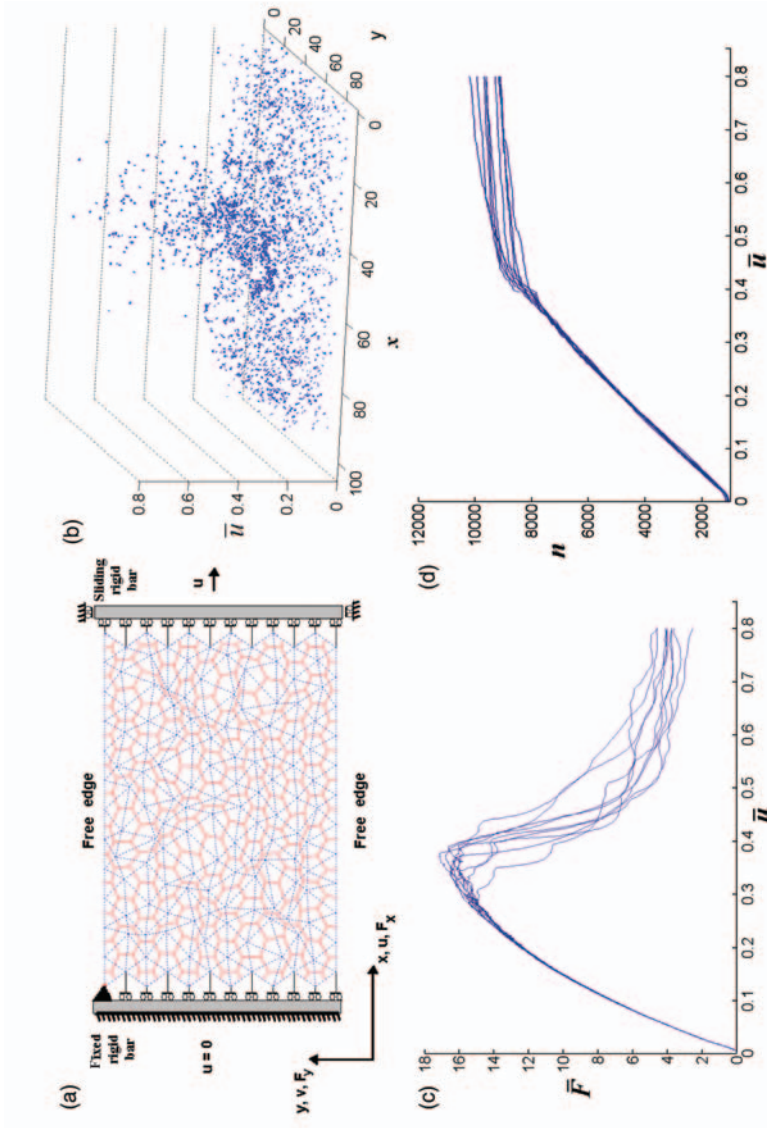
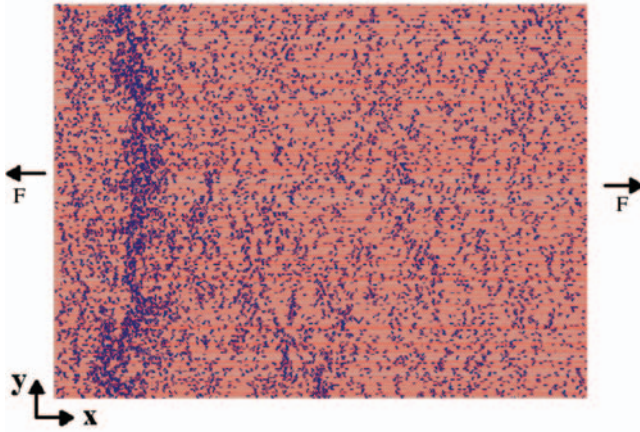


Figure 2. 12×12 Voronoi/Delaunay graph of the microstructure in tensile test configuration: (a), Location of broken bonds during a simulation; localization, and reduction of damage rate are evident after the transition; (b) F vs \bar{u} ; (c) n vs \bar{u} ; and (d) curves for the 10 replicates of $N = 192$.

Table 1. Number of runs per lattice size from MD simulations.

Size N	24	48	72	96	120	192
Replicates	100	34	30	25	20	13

**Figure 3.** Damage distribution with macrocrack at the threshold of failure for $N = 192$.

$N = (72, 120)$ are added and more than 10 runs are collected for smaller lattices. The simulation data are summarized in Table 1, for a total of more than 200 simulations.

Figure 2(b) shows the damage evolution and demonstrates that damage localization and reduced rupturing rate characterize the (homogeneous–heterogeneous) transition, i.e., the transition from damage nucleation to damage propagation. Figure 3 shows the damage distribution in a lattice with $N = 192$ at the threshold of failure. Diffuse uncorrelated damage from damage nucleation and macrocrack from damage localization are both evident. The evolution of the macrocrack can provide the ‘crack growth’ defined as ‘the interval of damage progression from the length below in which there is negligible POD to an allowable size determined by residual strength requirements’ (Goranson, 1993). The large variety of macrocrack patterns observed after damage localization are responsible for the broad data scatter in the softening phase (Figure 2(c) and (d)). The macrocrack that forms at the threshold of failure is the minimum growth resistance pattern and is random. The crack(s) tends to be more or less straight and orthogonal to the tensile direction, depending on the presence of local

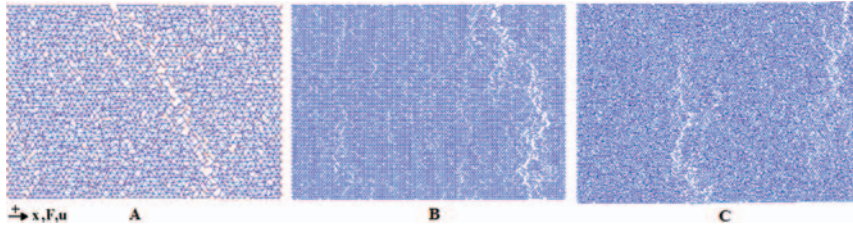


Figure 4. Failure patterns for lattice sizes $N = 24, 48, 96$ from the left.

energy ‘barriers,’ e.g., high-strength links close the propagating tips or shielding effects. Some failure patterns are shown in Figure 4.

PROBABILISTIC APPROACH: EXTREME VALUE THEORY

In the remaining part of the article an alternative empirical model is developed based on EVT, which deals with the application of the statistics of extremes. Gumbel (Gumbel, 1985) established EVT as a powerful mathematical tool used in engineering areas, such as structural engineering, ocean engineering, pollution and environmental engineering, highway design, electrical engineering, and strength of materials (Castillo, 1988). Extreme value theory (EVT) is a part of the more general theory of the ‘order statistics’.

By assuming x to be a random variable from a given population, $f(x)$ and $F(x)$ are the associated probability density function (*pdf*) and the cumulative distribution function (*cdf*), respectively. Also, assume that (X_1, X_2, \dots, X_n) is a random sample of size n from such a population and rearrange the observations in increasing order $(X_{1:n}, X_{2:n}, \dots, X_{n:n})$, with $X_{1:n} \leq X_{2:n} \leq \dots \leq X_{n:n}$. The r -th order statistic is defined as the member $X_{r:n}$ of the ordered collection of size n . Depending on the application, one or more order statistics can critically affect functionality, performances, or integrity of a complex system, and the statistical properties of $X_{r:n}$ drive design and maintenance activities. For example, if k waves of a height greater than a threshold h lead to failure of a breakwater barrier, the distribution of the $(n - k + 1)$ -th order statistic in a series of n waves observed at a given time period at a desired coastal location is a crucial design parameter to insure the reliability and durability of such barriers. Order statistics as a discipline can be used in this respect to determine the individual, joint, conditional probability of one or more order statistics from the parent functions $f(x)$ and $F(x)$ of the population to which the sample belongs. Only the case of independent and identically distributed (IID) random samples is considered here. If $m(r)$ is the number of elements in

$(X_{1:n}, X_{2:n}, \dots, X_{n:n})$, such that $X_{i:n} \leq x (i=1, \dots, r)$, then the event $(X_{r:n} \leq x)$ has *pdf* and *cdf* probability functions

$$f_{X_{r:n}}(x) = F^{r-1}(x) \cdot [1 - F(x)]^{n-r} \frac{f(x)}{B(r, n-r+1)}, \quad (1a)$$

$$F_{X_{r:n}}(x) = \sum_{k=r}^n \binom{n}{k} F^k(x) \cdot [1 - F(x)]^{n-k} = I_F(r, n-r+1), \quad (1b)$$

where $I_F(a, b)$ and $B(a, b)$ are the incomplete beta function and the beta function, respectively. The underlying idea for these results is that each X_i is a Bernoulli trial with only two possible outcomes: either $X_i \leq x$ (success) or $X_i \geq x$ (failure). In lieu of the IID hypothesis, the series of n trials follow a binomial distribution with success rate, $p = F(x)$. The probability $F_{X_{r:n}}(x)$, associated to $X_{r:n} \leq x$ is readily computed as the exceedance of at least r trials being successful, whereas the $f_{X_{r:n}}(x)$ in (1a) follows from (1b) by derivation with respect to x . Distribution-independent results, such as Equation (1) constitute the power of the theory of order statistics.

Distributions of Minima of Weibull Random IID Samples

Extreme value theory (EVT) has a more limited scope and is concerned with two order statistics only: the maximum and the minimum order statistics, i.e., the extremes defined as $X_{1:n} = \min(X_1, X_2, \dots, X_n)$ and $X_{n:n} = \max(X_1, X_2, \dots, X_n)$. In many applications, such as our failure problem, the statistics of either one of the two extremes is what matters. Weibull's theory is one of the first examples of EVT applied to structural engineering and allows inferring the strength of a full-size component or structure from the experimental data obtained in a laboratory with smaller specimens of the material. In this study, it is shown that EVT can be used to estimate the probability of failure of lattices at any scale once the properties are known at a smaller scale.

In a first-order approximation, the distribution of the first-order statistics (the minimum) is assumed to control the strength of the lattice. The distribution of random minima is obtained from Equations (1a) and (1b) by setting $r = 1$, which leads to the following *pdf* and *cdf*

$$f_{X_{1:n}}(x) = 1 - [1 - F(x)]^n, \quad (2a)$$

$$F_{X_{1:n}}(x) = n[1 - F(x)]^{n-1} f(x). \quad (2b)$$

The threshold of failure x , the sample size n (n is not the number of broken links anymore), and the parent *pdf* and *cdf* need to be specified. Simulation

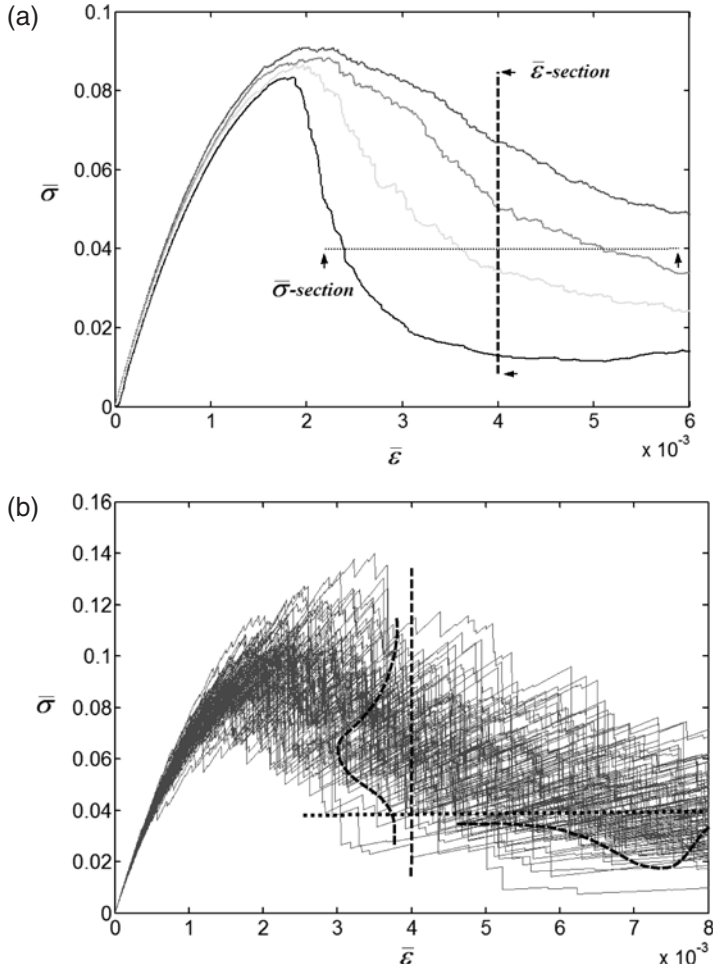


Figure 5. (a) Mean $\bar{\sigma} - \bar{\epsilon}$ curves and location of two orthogonal cross sections where the statistical properties are examined; (b) lattice responses of 100 samples for $N=24$.

data in Figure 5(a) show that the softening phase and failure are strongly dependent on lattice size. The problem consists of first determining the statistical properties of the data for the smallest lattice size $N=24$ and then inferring the same properties for larger size N . Figure 5(b) displays the macrostress responses of all 100 random replicates of size $N=24$. The statistical properties at each location $(\bar{\sigma}_0, \bar{\epsilon}_0)$ of the softening phase could be investigated by collecting the intersection points between the $\bar{\sigma} - \bar{\epsilon}$ curves and either the plane $\bar{\epsilon} = \bar{\epsilon}_0$ or the plane $\bar{\sigma} = \bar{\sigma}_0$. The choice of the section

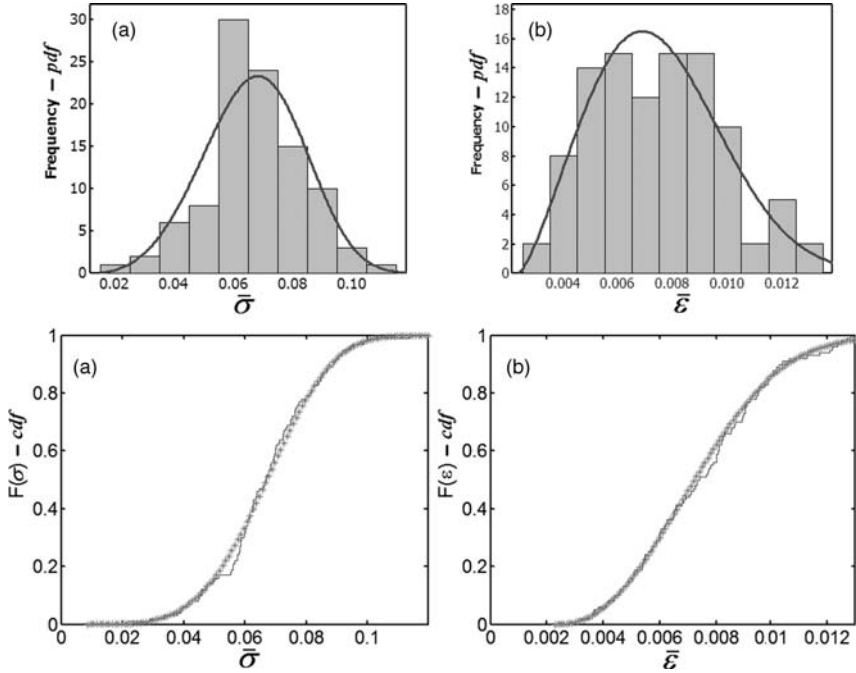


Figure 6. Histogram along with pdf and cdf from Weibull's fit for both ε -section: (a) and the σ -section (b) for $N = 24$.

plane depends on whether one is interested in the probability of a material to survive to a strain level $\bar{\varepsilon}_0$ or to a stress level $\bar{\sigma}_0$. Both cases are considered here. As shown in Figure 5, the sections are (arbitrarily) taken at $\bar{\varepsilon}_0 = 0.004$ and $\bar{\sigma}_0 = 0.04$. The frequency histograms for the two diagrams are shown in Figure 6(a) and 6(b) for the ε -section and the σ -section respectively.

The identification of the statistical distribution that fits the 100 observations in each sample is not a trivial task i.e., to determine what form of $f(x)$ and $F(x)$ to use in Equations (2a) and (2b). MINITAB 14© is used to screen out a set of continuous distributions, such as the normal, the lognormal, the Weibull, the gamma, the exponential, and others (MINITAB 14©). It is opportune to revise the formalism of statistical 'hypothesis testing' and the statistical techniques used for this analysis. The candidate distributions are fitted with the maximum likelihood (ML) method and the goodness-of-fit is assessed according to the Anderson-Darling (AD) test (MINITAB 14©, NIST/SEMATECH). Such a test is particularly well suited to compare the fit of competing distributions. The fit improves as the value

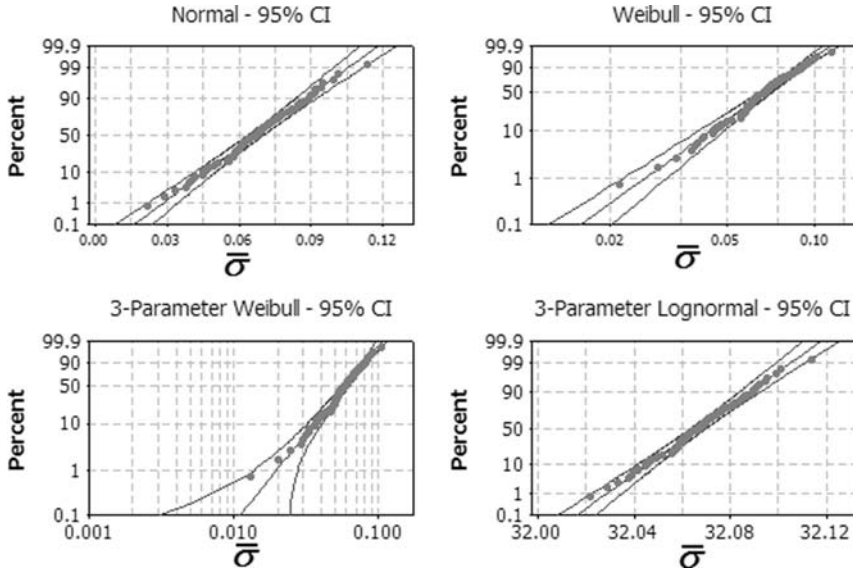


Figure 7. Identification of the statistical distribution for $\bar{\epsilon}_0 = 0.004$.

of the AD statistics reported on the probability plots (Figures 7 and 8) reduces. The AD statistical test is defined in (NIST/SEMATECH) as:

- H_0 : the data follow the specified distribution,
- H_1 : the data do not follow the specified distribution.

The ‘null hypothesis’ (H_0) is rejected (a candidate distribution is rejected) if the AD statistics is greater than a threshold value that depends on the distribution itself. In this case (H_1 is true), the test is customarily called significant. MINITAB does not report such a threshold value for AD but conveniently provides the corresponding P -value. Because of the way the AD test is formulated, the higher the P -value, the better the fit is. The P -value represents the lowest level of significance that leads to rejection of H_0 . The ‘significance’ α corresponds to the probability (chosen by the analyst) to reject H_0 when H_0 is true and, hence, commit an error (α -error). If P -value $< \alpha$, then H_0 is rejected in favor of H_1 . The choice of α depends on what hypothesis the analyst is interested in and on the criticality of the decision. A significance level of 20% ($\alpha = 0.2$) is conservative enough here to reject poor fitting. Figures 7 and 8 show the probability plots with 95% confidence limits of four candidate distributions, namely the Gaussian, the 3-parameters lognormal, and the 2 and 3-parameters Weibull. In all cases, the quality of fit is acceptable with P -value > 0.2 , as summarized in

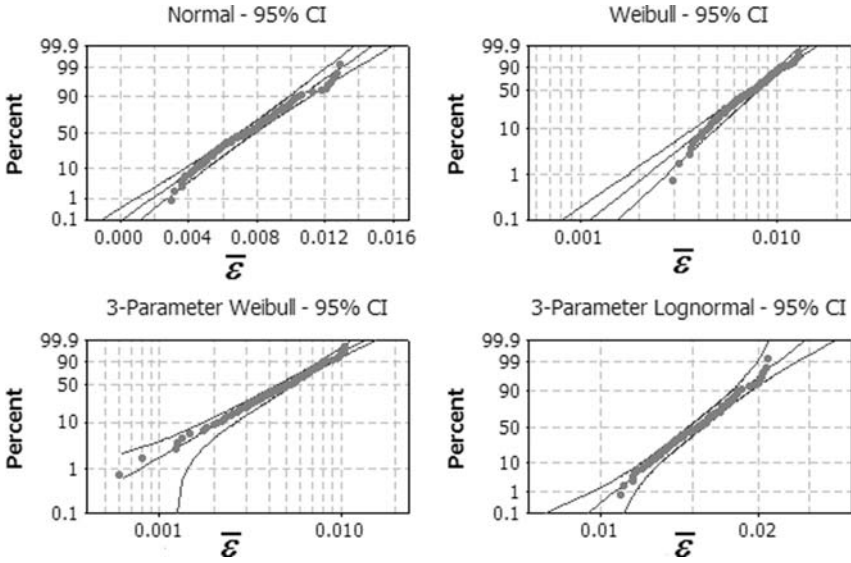


Figure 8. Identification of the statistical distribution for $\bar{\sigma}_0 = 0.04$.

Table 2. Goodness of fit statistics for the four distributions in Figures 7 and 8.

	$\bar{\sigma}$ -section		$\bar{\sigma}$ -section	
	P-value	AD-value	P-value	AD-value
Normal	0.661	0.273	0.364	0.396
Weibull	>0.250	0.416	>0.250	0.348
3-parameters Weibull	0.372	0.367	>0.500	0.218
Lognormal	>0.661	0.268	>0.250	0.304

Table 2. The minimal scatter of the data points around the straight lines provides the visual confirmation.

The choice is not obvious but the 3-parameters Weibull distribution (3-parameters to be omitted from now on) is finally selected for convenience. Such distribution offers great flexibility for the large variety of shapes that is capable to assume and, therefore, is one of the most widely used in failure analysis. Furthermore, the Weibull distribution exhibited superior performances in fitting the simulation data from the other lattice sizes. The theoretical justification underlying the Weibull distribution and related to the weak-link type of failure is also an appealing aspect. At last, the Weibull distribution is well suited for the EVT and leads to nice

analytical expressions. The *pdf* and *cdf* probability density function of the 3-parameters Weibull is,

$$f(x) = \frac{\gamma}{x - \beta} \left(\frac{x - \beta}{\alpha} \right)^\gamma e^{-((x-\beta)/\alpha)^\gamma} \quad (3a)$$

$$F(x) = 1 - e^{-((x-\beta)/\alpha)^\gamma}, \quad (3b)$$

where γ is the shape parameter, α the characteristic life, and β the shift or waiting time.

The *pdf* functions $f(x)$ for the ε -section and the σ -section are plotted on top of the histograms in Figure 6 (top). The *cdf* functions $F(x)$ are also shown in Figure 6 (bottom) together with the empirical *cdf* from simulation data. The estimates of the parameters from ML are $\gamma_\varepsilon = 3.929$, $\alpha_\varepsilon = 0.0064$, and $\beta_\varepsilon = 0.0087$ for the ε -section (Figure 6(a)), and $\gamma_\sigma = 2.3178$, $\alpha_\sigma = 0.0058$, and $\beta_\sigma = 0.0024$ for the σ -section (Figure 6(b)).

The above technique may provide a very detailed statistical description of the lattice properties but requires a large sample to identify the right distribution accurately. This approach yields ambiguous results when there are about 10 observations, as for $N = 192$, and is impossible when there is no sample at all, as in the case of a full-size structure. Instead, the knowledge of the properties for $N = 24$, can be combined with the EVT. By allowing the larger lattices of size $N = (48, 96, 192)$, to be subdivided into an integer number ‘ q ’ of lattices of size $N = 24$, the relation

$$q_i = \frac{L_i^2}{L_{24}^2} > 1 \quad (4)$$

is the ratio between the areas of the i -th large lattice and the $N = 24$, lattice $i = (48, 96, 192)$. The vector $\mathbf{q} = (4, 16, 64)$ is obtained from (4) in correspondence to $N = (48, 96, 192)$, through the approximation $L_i^2/L_{24}^2 \simeq N_i^2/N_{24}^2$, where $L = (N - 1)\ell$ and ℓ is the average link length. The q_i sub-lattices can be regarded as a random IID sample of size q_i . As depicted in Figure 2(b), damage nucleation is a random process independent of lattice size and affects the lattice area uniformly. The lattice is statistically homogeneous and each sub-domain constitutes a ‘representative volume element’ (Krajcinovic), where the damage evolves independently of the neighboring sub-domains. The interactions amongst sub-lattices become significant only in the vicinity of the force peak of the lattice response. The damage localization takes place when and where the ‘weakest’ sub-domain reaches the transition point. Afterwards, the surviving sub-domains in the vicinity of the damage localization are either shielded or subjected to a stress

level much higher than the net stress due to the stress concentration effect. Depending on the two cases, the neighboring sub-domains either become passive (shielding) or fail rapidly (stress concentration), without being able to contribute to the resistance of the overall lattice. Thus, the properties of a large lattice are expected to be entirely described by the statistics of minima of a sample size q_i . For the Weibull distribution, the *cdf* (Equation 1(b)) of the minima for $n = q_i$ can be rewritten as,

$$F_{1:n}(x) = 1 - e^{-n((x-\beta)/\alpha)^{\gamma}}, \quad (5)$$

by using Equations (3a) and (3b) as parent functions $f(x)$ and $F(x)$. The plots of $F_{1:n}(x)$ for $n = (4, 9, 16, 25, 64)$, i.e., $N = (48, 72, 96, 120, 192)$, are shown in Figures 9 and 10, together with experimental *cdf* from simulation data for comparison.

Accuracy of Results and Convergence

From the analysis of the data in Figures 9 and 10, the agreement between EVT and the numerical *cdf* is satisfactory for $N = (48, 72, 96, 120)$. Both ‘shape’ and ‘location’ of the theoretical *cdf* (Equation (5)) usually approximate well the numerical data. Mild deviations should be considered acceptable bearing in mind that most of the experimental *cdf* come from small samples of the order of 10 data points. Some concerns arise for the case $N = 192$ since there is a visible difference between predicted and numerical data for both $\bar{\varepsilon}$ -section (Figure 9) and $\bar{\sigma}$ -section (Figure 10). While the shapes look similar, the mismatch in ‘location’ is very evident especially for the $\bar{\varepsilon}$ -section data in Figure 9. This problem is likely related to the convergence of the numerical data in the softening data, which might be an issue for this type of analysis.

The $\bar{\sigma} - \bar{\varepsilon}$ response was generated by a molecular dynamic solver, which is an iterative explicit integration scheme. For large lattices, such as $N = 192$, the convergence to the quasi-static response becomes very slow in the softening regime. For the same tolerance level (expressed in total residual kinetic energy of the nodes), the convergence might not even occur after 50,000 iterations in the softening regime, while 5000 iterations are usually enough in the hardening phase. The choice of tolerance level is always a trade-off between feasibility (simulation time) and accuracy. A residual dynamic component is always to be expected to produce deviation of the $\bar{\sigma} - \bar{\varepsilon}$ response from the ‘true’ quasi-static trajectory. The reduced compliance in the softening phase makes the lattice less responsive towards applied stimuli and the deviations of the dynamic perturbation are much

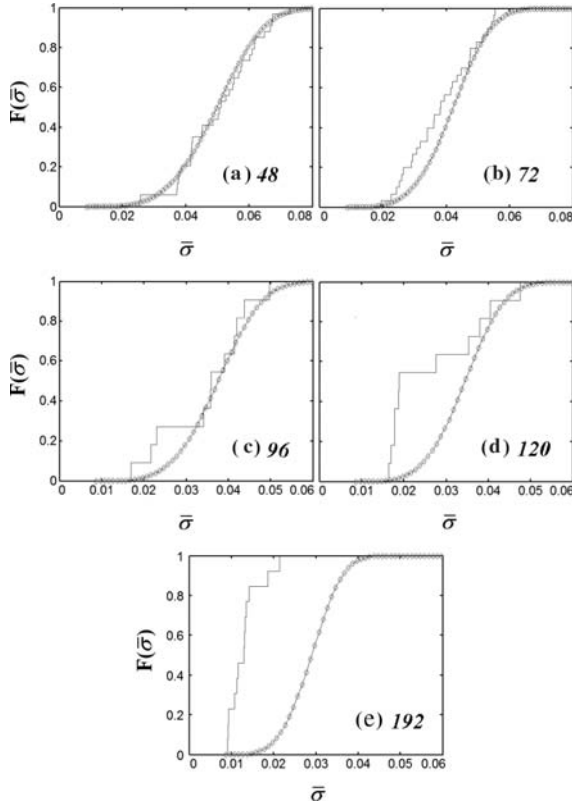


Figure 9. Predicted *cdf* of minima from EVT vs empirical *cdf* ($\bar{\epsilon}$ -section).

more pronounced than in hardening. This is particularly true for the fast descendent portion of the force response beyond the peak. The lack of accuracy introduces ‘bias’ into the experimental *cdf*, which explains the ‘location’ mismatch for $N=192$. These considerations hold for the other lattice sizes as well, but the bias becomes a problem for the largest microstructure.

In support of this justification, another sample of 10 random replicates was collected for $N=96$ by using a stricter tolerance level on the residual kinetic energy, about two orders of magnitude smaller than in the original simulations. Figure 11 plots the experimental *cdf* of both old (a) and new (b) samples. The new numerical data is more accurate and Table 3 reports the comparison between statistics.

The means and standard deviations tend to increase in the new simulations but the variation is sometimes minimal. However, in terms of

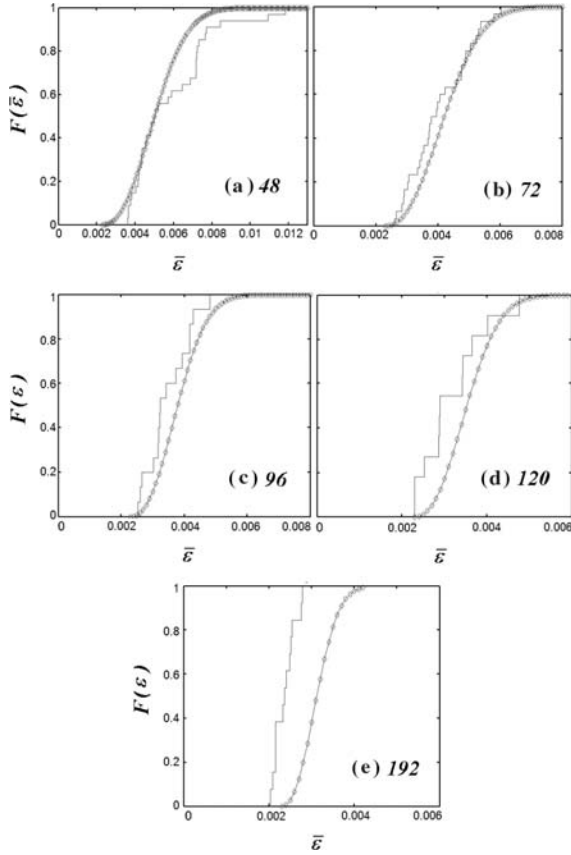


Figure 10. Predicted cdf of minima from EVT vs empirical cdf ($\bar{\sigma}$ -section).

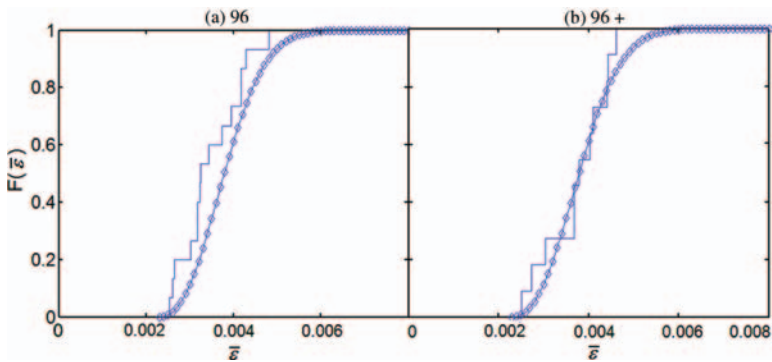


Figure 11. (a) Convergence issue for $N=96$. (b) higher convergence in improves the theory accuracy (only $\bar{\sigma}$ -section shown).

Table 3. Comparison between the original (old) sample and the more accurate one (new) for $N=96$.

	Old mean	New mean	Variation %	Old std. dev.	New std. dev.	Variation %
$\bar{\varepsilon}$ -section	0.0340	0.0348	$\sim +2.5$	0.0092	0.0102	$\sim +11$
$\bar{\sigma}$ -section	0.00348	0.00373	$\sim +7$	0.00068	0.00070	$\sim +3$

cdf, the new sample matches much better the theoretical predictions from EVT. More research is currently being conducted to further validate this argument and reach definitive conclusions.

Remarks and Applications

The results and previous discussion in support of the probabilistic model (5) mainly foster two conclusions for this section:

- (1) the EVT appears to work effectively in predicting the statistical property of the softening phase;
- (2) the bias (lack of accuracy) in the simulation data due to limited convergence can be misleading or fatal by a statistical analysis standpoint, even if the differences in the $\bar{\sigma} - \bar{\varepsilon}$ response are small.

The results of the EVT are extremely sensitive to the choice of the parent distributions and both form and fit of $f(x)$ must be correct (Gumbel, 1985). In this article, Equation (3) appeared appropriate.

The results have important applications. By repeating the analysis over the entire range of softening of $N=24$ and assuming that the same form of the distribution of the *pdf* is appropriate for such a range, one can obtain an empirical fit for the parameters $\{\gamma, \alpha, \beta\}$ in terms of the parameter $\bar{\varepsilon}_0$ or $\bar{\sigma}_0$ of the associated sectioning. Thus, if the $\bar{\varepsilon}$ -section is of interest, it is straightforward to derive the parametric expressions

$$f(\bar{\sigma}; \bar{\varepsilon}_0) = \frac{\gamma(\bar{\varepsilon}_0)}{\bar{\sigma} - \beta(\bar{\varepsilon}_0)} \left(\frac{\bar{\sigma} - \beta(\bar{\varepsilon}_0)}{\alpha(\bar{\varepsilon}_0)} \right)^{\gamma(\bar{\varepsilon}_0)} e^{-((\bar{\sigma} - \beta(\bar{\varepsilon}_0))/\alpha(\bar{\varepsilon}_0))^{\gamma(\bar{\varepsilon}_0)}}, \quad (6a)$$

$$F(\bar{\sigma}; \bar{\varepsilon}_0) = 1 - e^{-((\bar{\sigma} - \beta(\bar{\varepsilon}_0))/\alpha(\bar{\varepsilon}_0))^{\gamma(\bar{\varepsilon}_0)}}, \quad (6b)$$

from $\{\gamma(\bar{\varepsilon}_0), \alpha(\bar{\varepsilon}_0), \beta(\bar{\varepsilon}_0)\}$. Expressions (6) contain the full description of the softening regime for any lattice size. By inverting Equation (6b),

the expected value of the stress response $\hat{\sigma}(\bar{\varepsilon}_0, N)$ for a desired percentile $F_{1:n}(\hat{\sigma}, \bar{\varepsilon}_0) = \hat{F}$ is

$$\hat{\sigma}(\bar{\varepsilon}_0, N) = \left[1 - e^{-((\hat{\sigma}(\bar{\varepsilon}_0) - \beta(\bar{\varepsilon}_0)) / (\alpha(\bar{\varepsilon}_0)))^{\gamma(\bar{\varepsilon}_0)}} \right]^{-1} = \beta(\bar{\varepsilon}_0) + \left[-\frac{N_{24}}{N} \frac{\ln(1 - \hat{F})}{\alpha(\bar{\varepsilon}_0)} \right]^{1/\gamma(\bar{\varepsilon}_0)}, \quad (7)$$

which renders the softening an intrinsic property of the material. Similarly for the $\bar{\sigma}$ -section,

$$\hat{\varepsilon}(\bar{\sigma}_0, N) = \left[1 - e^{-((\hat{\varepsilon}(\bar{\sigma}_0) - \beta(\bar{\sigma}_0)) / (\alpha(\bar{\sigma}_0)))^{\gamma(\bar{\sigma}_0)}} \right]^{-1} = \beta(\bar{\sigma}_0) + \left[-\frac{N_{24}}{N} \frac{\ln(1 - \hat{F})}{\alpha(\bar{\sigma}_0)} \right]^{1/\gamma(\bar{\sigma}_0)}, \quad (8)$$

where $\{\gamma(\bar{\sigma}_0), \alpha(\bar{\sigma}_0), \beta(\bar{\sigma}_0)\}$ are required. The technical implication is that Equations (7) or (8) would allow a design with a desired level of survivability. The residual strength (allowable damage) $\hat{\sigma}$ for a failure life $\bar{\varepsilon}_0$ is readily available from Equation (7) and can be extrapolated for a large-size structure. For example, Figure 12 indicates that at $\bar{\varepsilon}_0 = 0.004$, the probability of failure for a stress level $\hat{\sigma} = 0.03$ is less than 5% for $N = 24$ and more than 50% for $N = 192$. Depending on the situation, either Equation (7) or (8) can be used as constitutive relations for the damage problem. The empirical approach is a powerful alternative to the mechanistic model, such as (Krajcinovic and Rinaldi, 2005a), based on the damage parameter.

CONCLUSIONS

This article is committed to constitutive modeling, failure, damage tolerance, and durability of structures, issues largely neglected in engineering practice and research (Goranson, 1993). The results offered in this article display the effectiveness of the statistical damage model reproducing data scatter in the softening regime and at failure. The numerical data produced with this approach could not be generated by classical continuum damage mechanics. Analytical semi-empirical models based on extreme value theory (EVT), i.e., Equations (7) and (8), can be derived in principle for the entire damage process and are viable design tools. Probabilistic models are not as rigorous as the analytical model but offer a more complete description of the statistical properties of the lattice response. This article

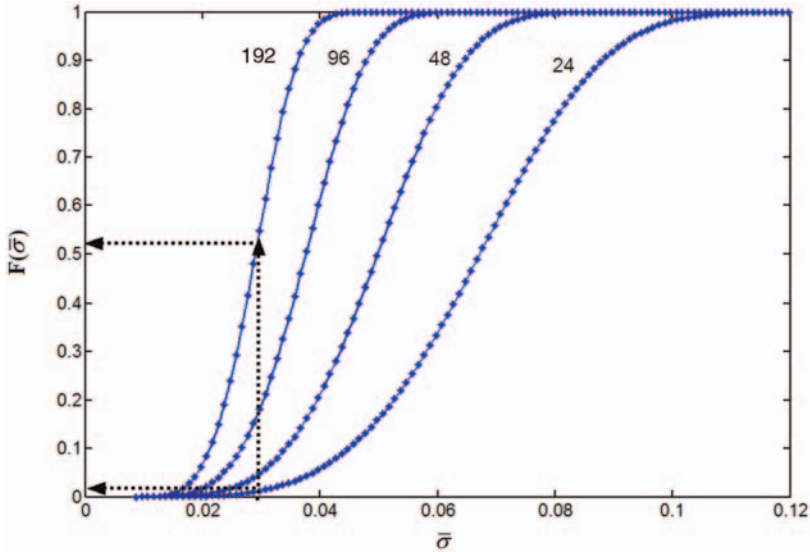


Figure 12. Predicted cdf at $\bar{\varepsilon}_0 = 0.004$ for $N = (24, 48, 96, 192)$ and comparison between probability of failure at $\hat{\sigma} = 0.03$ for $N = 24$ and $N = 192$.

outlines the importance of statistical methods, such as ordinary least squares, maximum likelihood, and testing hypothesis, for the selection of model parameters. These techniques are the basis for data-driven reasoning and decision-making in damage tolerance.

ACKNOWLEDGMENTS

This research is sponsored by the Mathematical, Information and Computational Science Division, Office of Advanced Scientific Computing Research, US Department of Energy under contract number DE-AC05-00OR22725 with UT-Battelle, LLC. The support of the Ministry of Science and Environmental Protection of Republic of Serbia to S. Mastilovic is gratefully acknowledged. The authors address a special thanks to Dr S. Simunovic at ORNL and Prof. Y.C. Lai at ASU for their valuable support.

REFERENCES

Castillo, C. (1988). *Extreme Value Theory in Engineering*, Academic Press, Inc., Boston.
 Davidge, R.W. (1979). *Mechanical Behavior of Ceramics*, Cambridge University Press, Cambridge, UK.

- Goranson, U.G. (1993). Damage Tolerance – Facts and Fiction, In: 14th *Plantema Memorial Lecture Presented at the 17th Symposium of the International on Aeronautical Fatigue*, Stockholm, Sweden.
- Gumbel, E.J. (1985). *Extreme Value Theory*, Columbia University Press., New York.
- Kachanov, L.M. (1958). On the Time to Failure under Creep Conditions, *Izv. AN SSSR, Ot. Tekhn. Nauk*, **8**: 26–31.
- Krajcinovic, D. and Rinaldi, A. (2005a). Statistical Damage Mechanics – 1 Theory, *J. of Applied Mechanics*, **72**: 76–85.
- Krajcinovic, D. and Rinaldi, A. (2005b). Thermodynamics and Statistical Physics of Damage Processes in Quasi-ductile Solids, *Mech. Mater.*, **37**: 299–315.
- Krajcinovic, D. Damage Mechanics, In: *North-Holland Series in Applied Mathematics and Mechanics*, Vol. 41, Elsevier, Amsterdam.
- Mastilovic, S. and Krajcinovic, D. (1999). Statistical Models of Brittle Deformation: Part II: Computer Simulations, *Int. J. Plasticity*, **15**: 427–456.
- MINITAB 14©, on-line manual.
- NIST/SEMATECH *e-Handbook of Statistical Methods*, <http://www.itl.nist.gov/div898/handbook/>, 2003.
- Rinaldi, A., Mastilovic, S. and Krajcinovic, D. (2005). Statistical Damage Mechanics – 2. Constitutive Relations, *J. of Applied Mechanics* (accepted).